Three-Dimensional Vortex Gyration Dynamics Unraveled by Time-Resolved Soft X-ray Laminography with Freely Selectable Excitation Frequencies

Simone Finizio,[*,†] Claire Donnelly,[‡,¶] Sina Mayr,[†,§] Ales Hrabec,[†,§] and Jörg Raabe[†]

†*Paul Scherrer Institut, 5232 Villigen PSI, Switzerland*

‡*Cavendish Laboratory, University of Cambridge, Cambridge CB3 0HE, United Kingdom*

¶*Max Planck Institute for Chemical Physics of Solids, 01187 Dresden, Germany*

§*Laboratory for Mesoscopic Systems, Department of Materials, ETH Zurich, 8093 Zurich, Switzerland*

E-mail: simone.finizio@psi.ch

Abstract

The imaging of magneto-dynamical processes has been, so far, mostly a two-dimensional business, due to the constraints of the available experimental techniques. In this manuscript, building on the recent developments of soft X-ray magnetic laminography, we present an experimental setup where magneto-dynamical processes can be resolved in all three spatial dimensions and in time at arbitrary frequencies. We employ this setup to investigate two resonant dynamical modes of a CoFeB microstructure, namely the fundamental vortex gyration mode and a magnetic field-induced domain wall excitation mode. For the former, we observe a large variation of the gyration dynamics

across the thickness of the core, coexisting with a breathing mode of the core. For the latter, we observe a uniform displacement of the domain walls across the thickness of the microstructure. The imaging of these two modes benchmarks the possibility to freely select the excitation frequency for soft X-ray time-resolved laminography, allowing for the investigation of resonant magneto-dynamical processes.

Keywords

magnetic vortex gyration, 3D time-resolved magnetic imaging, scanning transmission X-ray microscopy, laminography, magnetization dynamics

The investigation of three-dimensional magneto-dynamical processes has recently attracted attention thanks to their rich dynamical behavior and novel functionalities[1,2].

An example of such dynamical processes is given by the dynamics of magnetic vortex cores stabilized in thick ferromagnetic microstructures. In these thick microstructures, the interplay between exchange and magnetostatic energies leads to the stabilization of a "barrel" shaped vortex core, narrow at the top/bottom surfaces of the microstructure, and wider towards the center of the microstructure[3–5]. Magnetic vortex dynamics have been extensively investigated, both theoretically[6–10] and experimentally[11–15], including in non-trivial geometries[16,17]. As of now, however, no direct visualization of the three-dimensional dynamics of magnetic vortices has been performed.

Although, until recently, only indirect characterizations of three-dimensional magneto-dynamical processes could be performed[18,19], significant progress has been made towards three-dimensional imaging of magnetic systems, driven by the development of three-dimensional X-ray imaging techniques such as magnetic tomography[20] and laminography[21,22]. Of particular interest is the work reported in Ref.[21], where the dynamics of a 1.2 μm thick GdCo microstructure were, for the first time, resolved in all three dimensions. However, this groundbreaking study relied on the intrinsically pulsed structure of synchrotron radiation, investigating a dynamical process locked to the pulse repetition rate (500 MHz for Ref.[21])

to perform the time-resolved imaging. This is caused by the requirement to utilize a two-dimensional X-ray detector demanded by the ptychographic imaging technique used to acquire each projection[23]. Its limited bandwidth allows for the access to only integer multiples of the pulse repetition rate, directly impacting the ensemble of dynamical processes that can be investigated, as many such processes (such as e.g. magnetic vortex gyration) are resonant at particular frequencies. As a result, to fully probe magnetization dynamics in three dimensions, the free control over the frequency is key. In this work, we achieve frequency-flexible three-dimensional magnetic imaging through the combination of soft X-ray magnetic laminography with time-resolved scanning transmission X-ray microscopy (STXM) imaging, and we employ this technique for the investigation of the gyration dynamics of a barrel-like magnetic vortex structure stabilized in a thick ferromagnetic microstructured element.

In the laminographic imaging geometry, the sample rotation axis is not perpendicular to the imaging beam axis, but is rather oriented at a defined angle (in our case, 45°) with respect to the beam axis, as sketched in Fig. 1(a)[21–23]. While, in principle, there is no limitation on the orientation of the sample surface with respect to the laminography axis, in our case the sample surface is perpendicular to the laminography axis. This is due both to mechanical constraints (the plane defined by the stage used for the rotation of the sample), and as scanning the sample along the plane perpendicular to the laminography axis allows us to keep the sample surface always in the focal spot of the Fresnel zone plate used to focus the X-ray beam[22]. For thin film samples, the laminography geometry allows for the probing of a larger volume of the Fourier space compared to the tomographic imaging geometry (missing cone artifact against a missing wedge artifact[23]), improving the quality of the three-dimensional reconstruction. Furthermore, the rotation geometry is such that no changes in the effective thickness of the sample occur, simplifying the measurements[21–23]. Finally, laminography allows for the imaging of extended sample surfaces, as demonstrated in Ref.[23].

Compared to ptychographic imaging[21], STXM has the advantage of requiring a point detector. By using an avalanche photodiode (APD) with a bandwidth larger than the repetition

rate of the synchrotron light source (for the Swiss Light Source, 500 MHz), two consecutive X-ray pulses generated by the light source (separated by 2 ns) can be resolved by the APD. This allows for the possibility to sort each recorded photon count by the APD into separate time channels depending on the relative phase between when the count occurred and the excitation signal used to trigger the dynamical process, which is synchronized to a rational multiple of the X-ray pulse repetition rate[24]. This is achieved through a custom-designed field-programmable gate array (FPGA) setup. Thanks to this detection protocol, a larger comb of accessible frequencies, given by rational multiples of the master clock frequency, is available. Purely arbitrary excitation frequencies are still not accessible, but this final limitation can be easily lifted if time-of-arrival detection is performed[25].

To demonstrate the possibility of performing three-dimensional time-resolved imaging with freely selectable excitation frequencies, we performed time-resolved laminographic imaging of two spin dynamic modes of a 150 nm thick $Co_{40}Fe_{40}B_{20}$ (from now on referred to as CoFeB) 2.5×2.5 μm^2 microstructured square, which stabilizes a flux-closure magnetic Landau state at equilibrium. Before performing the time-resolved imaging, we acquired a static magnetic laminogram of the CoFeB microstructure. The reconstruction of the magnitude and orientation of the local magnetization vectors was performed using the algorithm described in Ref.[26]. The reconstructed image is shown in Fig. 2 (a) and (c). Here, the arrows depict the magnitude and orientation of the local magnetization vector, and are colored in a blue-white-red scale according to the x component of the vector. In addition to the reconstructed local magnetization vectors, we also show the vortex core, depicted as an isosurface of the z component (c_z) of the curl of the magnetization vector $\mathbf{c} = \nabla \times \mathbf{m}$ (see the Methodology section for additional details).

From the static magnetic laminogram, we can observe that the CoFeB microstructured square exhibits a magnetic uniaxial anisotropy along the x axis, which is evidenced by the larger area of the magnetic domains along the x axis and by the shape of the vortex core. In particular, the vortex core exhibits a S-shaped structure (in contrast to the one-dimensional

columnar barrel structure that would be expected in absence of anisotropy[3]) elongated along the anisotropy axis, with the vortex core meeting the top and bottom surfaces of the CoFeB microstructured square at two spots separated by a lateral distance of about 300 nm.

To qualitatively verify that the reconstructed laminogram resembles the expected magnetic configuration, three-dimensional micromagnetic simulations of the CoFeB microstructured square with anisotropy, the value of which was determined from magneto-optical Kerr effect measurements, were performed with the finite-differences simulation package MuMax3[27] (details about the simulations can be found in the Methodology section). The simulated three-dimensional magnetic configuration is shown in Figs. 2(b) and (d), where its close resemblance to the experimental data can be observed.

Having determined the static magnetic configuration of the CoFeB microstructure, we next investigate its dynamics by performing time-resolved magnetic laminography. Specifically, by injecting a microwave signal across a Cu microantenna fabricated on top of the CoFeB microstructure, a set of different magneto-dynamical modes can be excited, ranging from the gyration of the vortex core to the excitation of the magnetic domain walls, and to the emission and propagation of spin waves. For this work, we performed three-dimensional time-resolved imaging of the fundamental vortex gyration mode (frequency of 326 MHz) and of a magnetic field-induced domain wall excitation mode (frequency of 913 MHz). The experimental setup employed for the time-resolved measurements is sketched in Fig. 1(b) and described in more detail in the Methodology section.

Figure 3 shows snapshots of the reconstructed magnetization profile for the domain wall excitation and vortex core gyration modes. As for the static laminogram presented in Fig. 2, we again show the reconstructed magnitude and orientation of the local magnetic moments and the isosurfaces of the z component of the curl of the magnetization, c_z. For the domain wall excitation mode (Fig. 3(a)), we show a set of isosurfaces of c_z, which allow us to delineate the magnetic domain walls of the CoFeB microstructure while, for the vortex gyration mode, we show the isosurface delineating the vortex core. Furthermore, for each of the snapshots

depicted in Figs. 3(a-b), we show the change in c_z with respect to its average value across one cycle of excitation, which allows us to visualize the motion of the magnetic domain walls in Fig. 3(a) and of the vortex core in Fig. 3(b).

In addition, by determining the magnitude of the change in the in-plane angle of the magnetization across one cycle of excitation for each voxel of the time-resolved laminogram, the spatial localization of the two modes can be determined. This is depicted in Fig. 3(c) for an excitation frequency of 913 MHz, where it can be observed that the mode is localized in the domain walls of the CoFeB square, allowing it to be identified as a domain wall excitation mode. For the excitation at 326 MHz, shown in Fig. 3(d), the mode is primarily localized in the vortex core, allowing it to be identified as a vortex gyration mode.

One of the main advantages of time-resolved laminographic imaging is that it allows us to resolve differences in the dynamics through the depth of a structure, and this can be well observed comparing the two magneto-dynamical modes shown in Fig. 3. In particular, the vortex core gyration mode exhibits a strong variation of its dynamics across its thickness, while the domain wall excitation mode exhibits a practically uniform motion along the thickness of the CoFeB microstructure. For the domain wall excitation mode (Fig. 3(a)), a precession of the magnetization within the domain wall can be observed. This precession, visible by the changes in the position of the c_z isosurfaces across one cycle of excitation, is predominantly uniform along the thickness of the microstructure. Therefore, while the possibility to measure this domain wall excitation mode provides a demonstration of the free selection of the excitation frequency, for the remainder of this work we will concentrate on the vortex gyration mode (Fig. 3(b)), where the laminographic imaging allows for the unraveling of the three-dimensional vortex core dynamics.

The injection of the 326 MHz RF signal excites the gyration of the vortex core, as shown in Fig. 3(b). A strong variation of its dynamical behavior across the thickness of the CoFeB microstructure can be observed.

To obtain more insight into the three-dimensional dynamics of the vortex core, we tracked

the position of its center of mass across each slice of the time-resolved image, as shown in Fig. 4(a). We then calculated the amplitude of the core's gyration in the $x-y$ plane at each slice, as shown in Fig. 4(b). The highest amplitude in the $x-y$ core's gyration occurs at the top and bottom surfaces of the CoFeB square, where the core is perpendicular to the $x-y$ plane, and the motion of the center of mass of the vortex core is elliptical, with its major axis along the easy axis of the uniaxial anisotropy (i.e. along x). At the top and bottom surfaces of the microstructure, the major axis of the ellipse fitting the vortex core motion is of about 30 nm, while the minor axis is of about 10 nm. Towards the center of the core, the eccentricity of its motion reduces, as shown by the reduction of the major axis of the ellipse to about 20 nm. These measurements show that the technique can resolve nanometric dynamics. Furthermore, the experimental results are also be well-reproduced by micromagnetic simulations, as shown in Figs. 4(c) and (d).

The gyrotropic motion of the vortex core is also paired with a breathing mode of the core, i.e. an expansion and contraction of the vortex core volume. The breathing of the vortex core can be visualized by determining the volume enclosed by a given isosurface of c_z for each time step. The specific isosurface has been selected to be equal to 90% of the maximum of c_z, and allows for the determination of the relative change in the vortex core volume across one cycle of excitation. Such time dependence is shown in Fig. 5(a), and the corresponding micromagnetic simulations qualitatively confirming the experimental data are shown in Fig. 5(b). Note here that the discretization grid utilized in the micromagnetic simulations affects the magnitude of the calculated curl, which can affect the quantitative agreement between the simulations and the experimental data.

The coexistence of gyration and breathing, coupled with the three-dimensional structure of the vortex core at its equilibrium configuration provides an additional energy reservoir if compared to two dimensional vortex cores. For such three-dimensional vortex cores, this additional energy reservoir requires a generalization of the Thiele model, where a magnetic inertial mass term has to be included[12,28,29]. Through time-resolved laminographic imaging,

the three-dimensional dynamical deformation of topological objects such as magnetic vortex cores can therefore be directly imaged, providing a direct experimental verification of predictions e.g. from micromagnetic simulations. This imaging protocol will also allow to reduce the exclusive reliance on micromagnetics for insights into three-dimensional dynamics, and offer the possibility to directly observe dynamical behaviors not predicted by micromagnetic simulations.

In conclusion, we have presented a time-resolved setup based on X-ray laminography combined with time-resolved STXM imaging that allows for the investigation of three-dimensional magneto-dynamical processes with the possibility to freely select the excitation frequency. This will allow for the possibility to resolve a range of resonant magnetization dynamic processes in three-dimensions, such as e.g. the generation, propagation, and localization of spin waves, domain wall motion dynamics, dynamics of three-dimensional topological objects such as hopfions, and the investigation of three-dimensional magnetic nanostructures. In particular, we have demonstrated here the three-dimensional mapping of two different dynamic modes of a microstructured CoFeB square stabilizing a Landau flux closure state. The two modes are the gyration of the vortex core, excited at 326 MHz, and the motion of the domain walls of the Landau pattern, excited at 913 MHz. The two investigated modes show a substantially different behavior along the thickness of the CoFeB square, with the domain wall excitation mode displacing uniformly along the thickness, and the vortex core gyration mode exhibiting a strongly non-uniform behavior along its thickness, which is further enhanced by the uniaxial anisotropy of the CoFeB microstructure. For this mode, the gyration of the vortex core is coexisting with a breathing of the vortex core, indicating that energy can be stored in the deformation of the core itself.

As a final note, it should be considered that, for time-resolved laminography imaging, a set of projections has to be acquired in order to reconstruct the three-dimensional magnetization configuration. Due to the large number of projections, a time-resolved laminography image currently requires a considerable investment in measurement time. Nonetheless, thanks to

the planned upgrades of several synchrotrons towards diffraction limited sources, the future of time-resolved laminography imaging is bright: improvements in the intensity, brilliance, and coherence of the X-ray beam produced by diffraction limited source will allow for the reduction of integration times of several factors.

Methodology

In this section, a summary of the methodology utilized for the work presented in this manuscript will be presented. Detailed methodology information is presented in the supporting information.

Sample fabrication

Microstructured CoFeB squares (2.5 μm wide, 150 nm thick) were patterned on top of a 200 nm thick, 1×1 mm^2 wide Si_3N_4 membrane on a 5×5 mm^2, 250 μm thick, intrinsic Si frame by electron beam lithography followed by liftoff. The CoFeB film was deposited by DC magnetron sputtering. On top of the CoFeB microstructure, a 5 μm wide, 300 nm thick, Cu stripline was fabricated by electron beam lithography followed by liftoff. The Cu film was deposited by thermal evaporation.

Time-resolved soft X-ray laminography

The three-dimensional time-resolved images were acquired through laminographic imaging[23], where each two-dimensional projection was acquired by STXM imaging. The X-ray energy was tuned to the L_2 edge of Cobalt (ca. 793 eV). The laminography angle was selected to be 45°. A total of 50 projections were acquired for each time-resolved image, yielding a theoretical z resolution of 10 nm[23]. For each projection, three time-resolved STXM images were acquired, two with circular polarization of opposite helicities and the third with linear polarization. This allows for the correction of discrepancies in the degree of circular

polarization between the two helicities[22,30].

Each time-resolved STXM image is composed of 7 binned frames. The dynamics are excited by injecting a RF current across the Cu stripline, generating an oscillating magnetic field along the x axis. The electrical circuit is schematically depicted in Fig. 1(b).

The reconstruction of the three-dimensional magnetic configuration was performed for each of the 7 frames according to the process described in[21,22]. The final three-dimensional time-resolved images were rendered using the free software Paraview[31]. To visualize the vortex core, we show the magnitude of the z component, c_z, of the curl of the magnetization $\mathbf{c} = \nabla \times \mathbf{m}$[21]. The position and volume of the vortex core was determined by calculating the center of mass and the volume of the region enclosed by the $c_z = 0.9 \times \max(c_z)$ isosurface for each z slice of the time-resolved laminography image.

Micromagnetic simulations

Micromagnetic simulations of the CoFeB microstructured square presented here were performed using the finite differences MuMax^3 framework[27]. A three-dimensional simulation grid was considered, consisting of a $512 \times 512 \times 32$ px^3 lattice with a $4.88 \times 4.88 \times 4.68$ nm^3 cell. A saturation magnetization of $M_s = 10^6$ A m^{-1}, an exchange stiffness of $A_{ex} = 10^{-11}$ J m^{-1}, a Gilbert damping constant of $\alpha = 0.05$, and a uniaxial anisotropy of 5 kJ m^{-3} along the x axis were used. A sinusoidal magnetic field of 5 mT along the x direction was then applied, reproducing the experimental configuration. Note here that the parameters for the micromagnetic simulations were not fine tuned, as the aim of the micromagnetic simulations was to show their qualitative agreement with the experimental data.

Author Contributions

SF conceived the experiment with input from CD and JR. SF and JR implemented the time-resolved laminography setup. SF designed the sample and performed the lithographical

patterning. AH deposited the CoFeB films. SF, SM, CD, and AH performed the time-resolved laminography experiments and interpreted the resulting data, using code provided by CD. SF performed the micromagnetic simulations. SF wrote the manuscript, with input from all authors.

Competing Interests

The authors declare no competing financial interests.

Data availability

The data that support the conclusions of this work are available on the following public repository [[link provided upon publication]].

Acknowledgement

This work was performed at the PolLux (X07DA) endstation of the Swiss Light Source, Paul Scherrer Institut, Villigen PSI, Switzerland. The research leading to these results has received funding from the Swiss National Science Foundation under grant agreement No. 172517. The PolLux endstation was financed by the German Bundesministerium für Bildung und Forschung through contracts 05K16WED and 05K19WE2. C.D. acknowledges support from the Max Planck Society Lise Meitner Excellence Program.

Supporting Information Available

The following supporting information is available:

- **SupplementaryInformation.pdf** - Supplementary information, including detailed methodology.

- **DomainWallExcitation_Isosurfaces.avi** - Video displaying the change in the spin configuration and the motion of the magnetic domain walls for the domain wall excitation mode (913 MHz). The video is shown in the same perspective as for Fig. 3(a). Here, the isosurfaces marking the position of the domain wall are shown.

- **DomainWallExcitation_CurlDifference.avi** - Video displaying the change in the spin configuration and the motion of the magnetic domain walls for the domain wall excitation mode (913 MHz). The video is shown in the same perspective as for Fig. 3(a). Here, the changes in the c_z component are shown.

- **VortexGyration_Isosurfaces.avi** - Video displaying the change in the spin configuration and the deformation of the vortex core for the vortex core gyration mode (326 MHz). The video is shown in the same perspective as for Fig. 3(b). Here, the isosurface marking the position of the vortex core is shown.

- **VortexGyration_CurlDifference.avi** - Video displaying the change in the spin configuration and the deformation of the vortex core for the vortex core gyration mode (326 MHz). The video is shown in the same perspective as for Fig. 3(b). Here, the changes in the c_z component are shown.

References

(1) Fernandez-Pacheco, A.; Streubel, R.; Fruchart, O.; Hertel, R.; Fischer, P.; Cowburn, R. P. Three-dimensional Nanomagnetism. *Nature Communications* **2017**, *8*, 15756.

(2) Fischer, P.; Sanz-Hernandez, D.; Streubel, R.; Fernandez-Pacheco, A. Launching a new Dimension with 3D Magnetic Nanostructures. *APL Materials* **2020**, *8*, 010701.

(3) Usov, N. A.; Peschany, S. E. Magnetization curling in a fine cylindrical particle. *Journal of Magnetism and Magnetic Materials* **1993**, *118*, L290.

(4) Hubert, A.; Schäfer, R. *Magnetic Domains: The Analysis of Magnetic Microstructures*; Springer Verlag, 1998.

(5) Fischer, P.; Im, M.-Y.; Kasai, S.; Yamada, K.; Ono, T.; Thiaville, A. X-ray imaging of vortex cores in confined magnetic structures. *Physical Review B* **2011**, *83*, 212402.

(6) Thiele, A. Steady-State Motion of Magnetic Domains. *Physical Review Letters* **1974**, *30*, 230.

(7) Roy, P. In-plane anisotropy control of the magnetic vortex gyrotropic mode. *Applied Physics Letters* **2013**, *102*, 162411.

(8) Krüger, B.; Drews, A.; Bolte, M.; Merkt, U.; Pfannkuche, D.; Meier, G. Harmonic oscillator model for current- and field-driven magnetic vortices. *Physical Review B* **2007**, *76*, 224426.

(9) Zarzuela, R.; Chudnovsky, E. M.; Tejada, J. Excitation modes of vortices in submicron magnetic disks. *Physical Review B* **2013**, *87*, 014413.

(10) Ben Youssef, J.; Vukadinovic, N.; Billet, D.; Labrune, M. Calculation of three-dimensional magnetic normal modes in mesoscopic permalloy prisms with vortex structure. *Physical Review B* **2007**, *76*, 094407.

(11) Guslienko, K. Y. Low-frequency vortex dynamic susceptibility and relaxation in mesoscopic ferromagnetic dots. *Applied Physics Letters* **2006**, *89*, 022510.

(12) Guslienko, K. Y.; Kakazei, G. N.; Ding, J.; Liu, X. M.; Adeyeye, A. O. Giant moving vortex mass in thick magnetic nanodots. *Scientific Reports* **2015**, *5*, 13881.

(13) Finizio, S.; Wintz, S.; Kirk, E.; Suszka, A. K.; Gliga, S.; Wohlhüter, P.; Zeissler, K.; Raabe, J. Control of the gyration dynamics of magnetic vortices by the magnetoelastic effect. *Physical Review B* **2017**, *96*, 054438.

(14) Noske, M.; Gangwar, A.; Stoll, H.; Kammerer, M.; Sproll, M.; Dieterle, G.; Weigand, M.; Fähnle, M.; Woltersdorf, G.; Back, C. H.; Schütz, G. Unidirectional sub-100-ps magnetic vortex core reversal. *Physical Review B* **2014**, *90*, 104415.

(15) Ding, J.; Kakazei, G. N.; Liu, X.; Guslienko, K. Y.; Adeyeye, A. O. Higher order vortex gyrotropic modes in circular ferromagnetic nanodots. *Scientific Reports* **2014**, *4*, 4796.

(16) Bublikov, K.; Tobik, J.; Sadovnikov, A. V.; Mruczkiewicz, M. Vortex gyrotropic mode in curved nanodots. *Journal of Magnetism and Magnetic Materials* **2021**, *537*, 168105.

(17) Ding, J.; Jain, S.; Lapa, P. N.; Khaire, T.; Lendinez, S.; Posada, C. M.; Zhang, W.; Pearson, J. E.; Hoffmann, A.; Novosad, V. Gyrotropic frequency control in ferromagnetic dots using a nanoscale vortex barrier. *AIP Advances* **2016**, *6*, 056102.

(18) Wartelle, A.; Trapp, B.; Stano, M.; Thirion, C.; Bochmann, S.; Bachmann, J.; Foerster, M.; Aballe, L.; Mentes, T. O.; Locatelli, A.; Sala, A.; Cagnon, L.; Toussaint, J.-C.; Fruchart, O. Bloch-point-mediated topological transformations of magnetic domain walls in cylindrical nanowires. *Physical Review B* **2019**, *99*, 024433.

(19) Mayr, S.; Flajsman, L.; Finizio, S.; Hrabec, A.; Weigand, M.; Förster, J.; Stoll, H.; Heyderman, L. J.; Urbanek, M.; Wintz, S. Spin-Wave Emission from Vortex Cores under Static Magnetic Bias Fields. *Nano Letters* **2021**, *21*, 1584.

(20) Donnelly, C.; Guizar-Sicarios, M.; Scagnoli, V.; Gliga, S.; Holler, M.; Raabe, J.; Heyderman, L. J. Three-dimensional magnetization structures revealed with X-ray vector nanotomography. *Nature* **2017**, *547*, 328.

(21) Donnelly, C.; Finizio, S.; Gliga, S.; Holler, M.; Hrabec, A.; Odstrcil, M.; Mayr, S.; Scagnoli, V.; Heyderman, L. J.; Guizar-Sicarios, M.; Raabe, J. Time-resolved imaging of three-dimensional nanoscale magnetization dynamics. *Nature Nanotechnology* **2020**, *15*, 356.

(22) Witte, K.; Späth, A.; Finizio, S.; Donnelly, C.; Watts, B.; Sarafimov, B.; Odstrcil, M.; Guizar-Sicarios, M.; Holler, M.; Fink, R. H.; Raabe, J. From 2D STXM to 3D imaging: soft X-ray laminography of thin specimens. *Nano Letters* **2020**, *20*, 1305.

(23) Holler, M.; Odstrcil, M.; Guizar-Sicarios, M.; Lebugle, M.; Müller, E.; Finizio, S.; Tinti, G.; David, C.; Zusman, J.; Unglaub, W.; Bunk, O.; Raabe, J.; Levi, A. F. J.; Aeppli, G. Three-dimensional imaging of integrated circuits with macro- to nanoscale zoom. *Nature Electronics* **2019**, *2*, 464.

(24) Puzic, A.; Korhonen, T.; Kalantari, B.; Raabe, J.; Quitmann, C.; Jüllig, P.; Bommer, L.; Goll, D.; Schütz, G.; Wintz, S.; Strache, T.; Körner, M.; Marko, D.; Bunce, C.; Fassbender, J. Photon Counting System for Time-resolved Experiments in Multibunch mode. *Synchrotron Radiation News* **2010**, *23*, 26.

(25) Finizio, S.; Mayr, S.; Raabe, J. Time-of-arrival detection for time-resolved scanning transmission X-ray microscopy imaging. *Journal of Synchrotron Radiation* **2020**, *27*, 1320.

(26) Donnelly, C.; Gliga, S.; Scagnoli, V.; Holler, M.; Raabe, J.; Heyderman, L. J.; Guizar-Sicarios, M. Tomographic reconstruction of a three-dimensional magnetization vector field. *New Journal of Physics* **2018**, *20*, 083009.

(27) Vansteenkiste, A.; Leliaert, J.; Dvornik, M.; Helsen, M.; Garcia-Sanchez, F.; Van Waeyenberge, B. The design and verification of MuMax3. *AIP Advances* **2014**, *4*, 107133.

(28) Makhfudz, I.; Krüger, B.; Tchernyshyov, O. Inertia and Chiral Edge Modes of a Skyrmion Magnetic Bubble. *Physical Review Letters* **2012**, *109*, 217201.

(29) Büttner, F. et al. Dynamics and inertia of skyrmionic spin structures. *Nature Physics* **2015**, *11*, 225.

(30) Raabe, J.; Tzvetkov, G.; Flechsig, U.; Böge, M.; Jaggi, A.; Sarafimov, B.; Vernooij, M. G. C.; Huthwelker, T.; Ade, H.; Kilcoyne, D.; Tyliszczak, T.; Fink, R. H.; Quitmann, C. PolLux: A new facility for soft x-ray Spectromicroscopy at the Swiss Light Source. *Review of Scientific Instruments* **2008**, *79*, 113704.

(31) Ahrens, J.; Geveci, B.; Law, C. *ParaView: an end-user tool for large data visualization*; Elsevier, 2005.

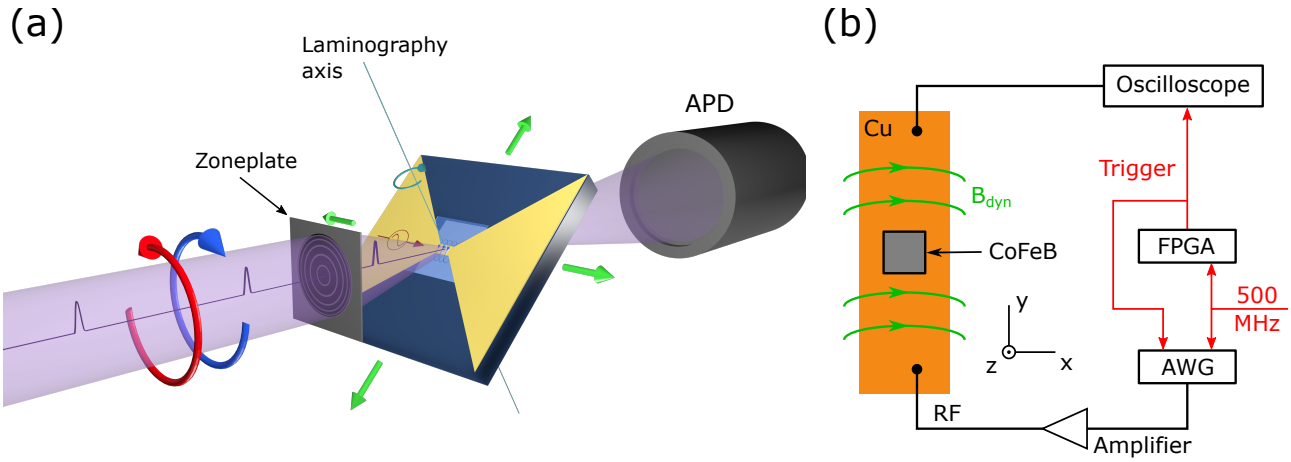

Figure 1: (a) Sketch of the laminography imaging setup. The sample is mounted under an angle of 45° (corresponding to the laminography rotation axis) with respect to the X-ray beam. (b) Electrical configuration utilized for the excitation of the dynamical processes presented here. An arbitrary waveform generator (AWG), frequency locked to the 500 MHz master clock of the synchrotron light source, is used to inject a RF current across a stripline fabricated above a $Co_{40}Fe_{40}B_{20}$ microstructured square, giving rise to an oscillating magnetic field along the x axis. The red signals indicate synchronization and timing signals.

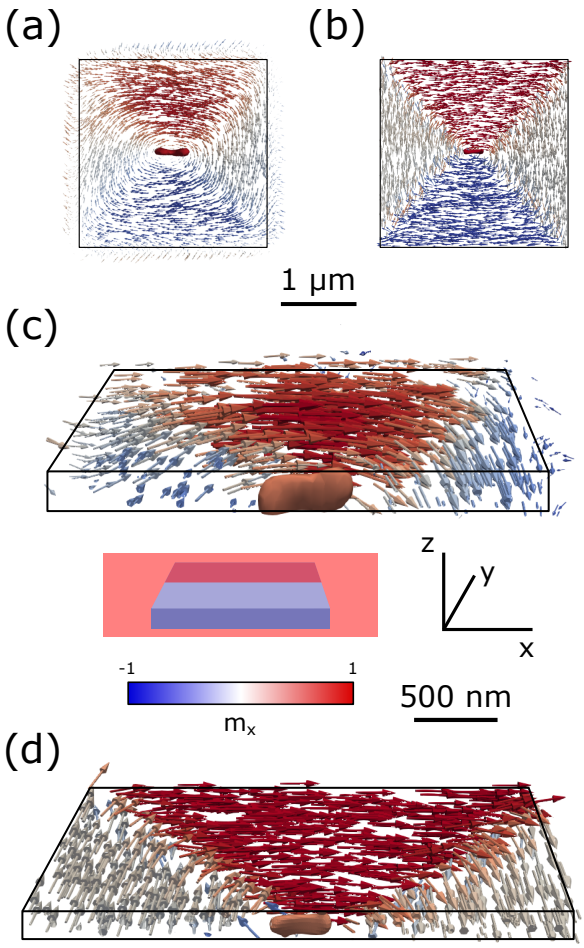

Figure 2: Static magnetic configuration of the CoFeB microstructure. (a) Top view of the reconstructed magnetic configuration, and (b) corresponding micromagnetic simulation. (c) Section of the measured laminogram along the the sectioning plane depicted below the image, and (d) corresponding micromagnetic simulation.

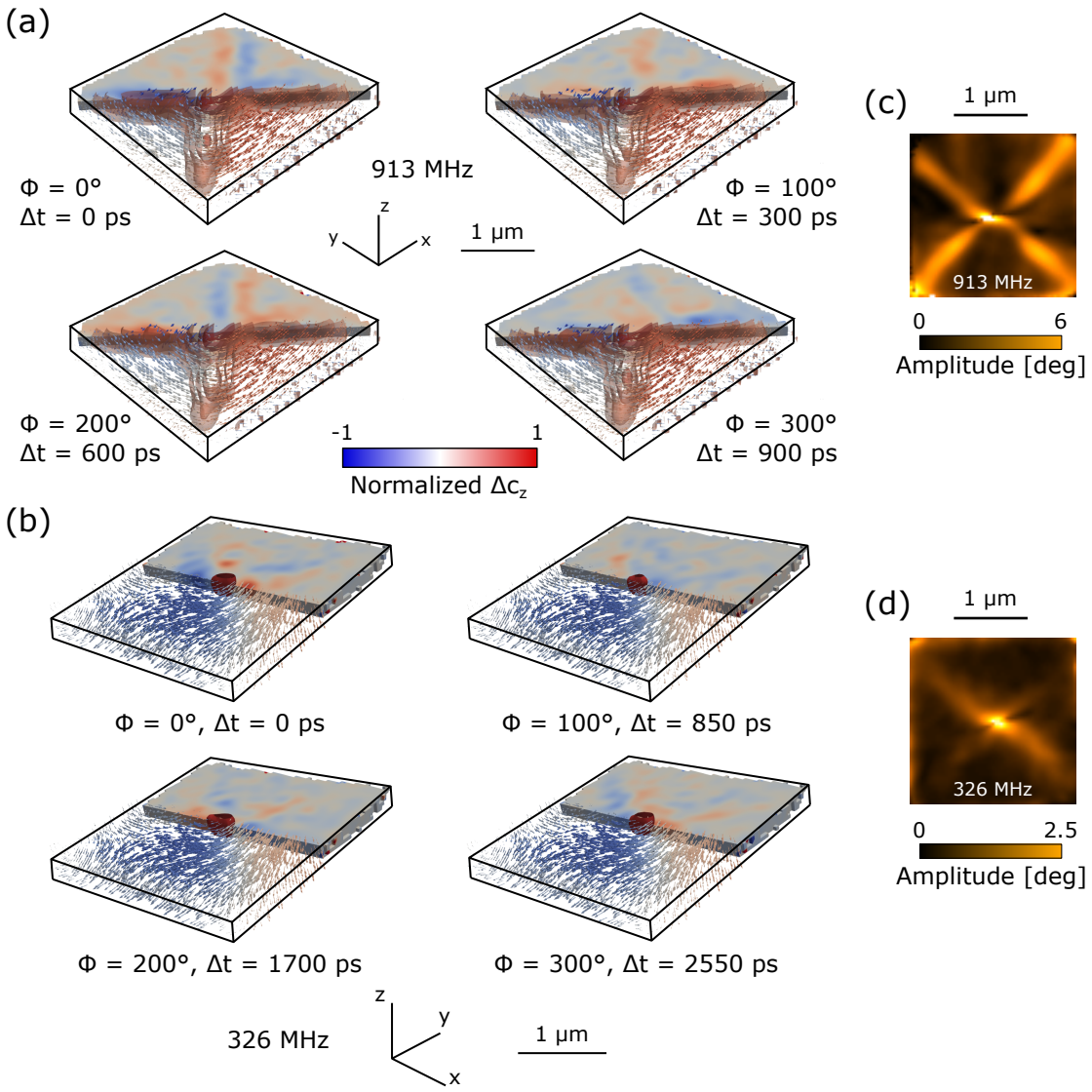

Figure 3: Three-dimensional single-frame renderings of the time-resolved magnetic laminograms at excitation frequencies of (a) 913 MHz and (b) 326 MHz. Φ indicates the phase of the excitation signal probed by each snapshot. For (a), the red isosurfaces of c_z follow the domain walls. For the snapshots pictured in (b), the vortex core is shown by the red isosurface of c_z. For both the (a) and (b) panels, the change in c_z with respect to its average value across one cycle of excitation is shown. Panels (c) and (d) visualize the areas, where the two modes (913 MHz for (c) and 326 MHz for (d)) are localized.

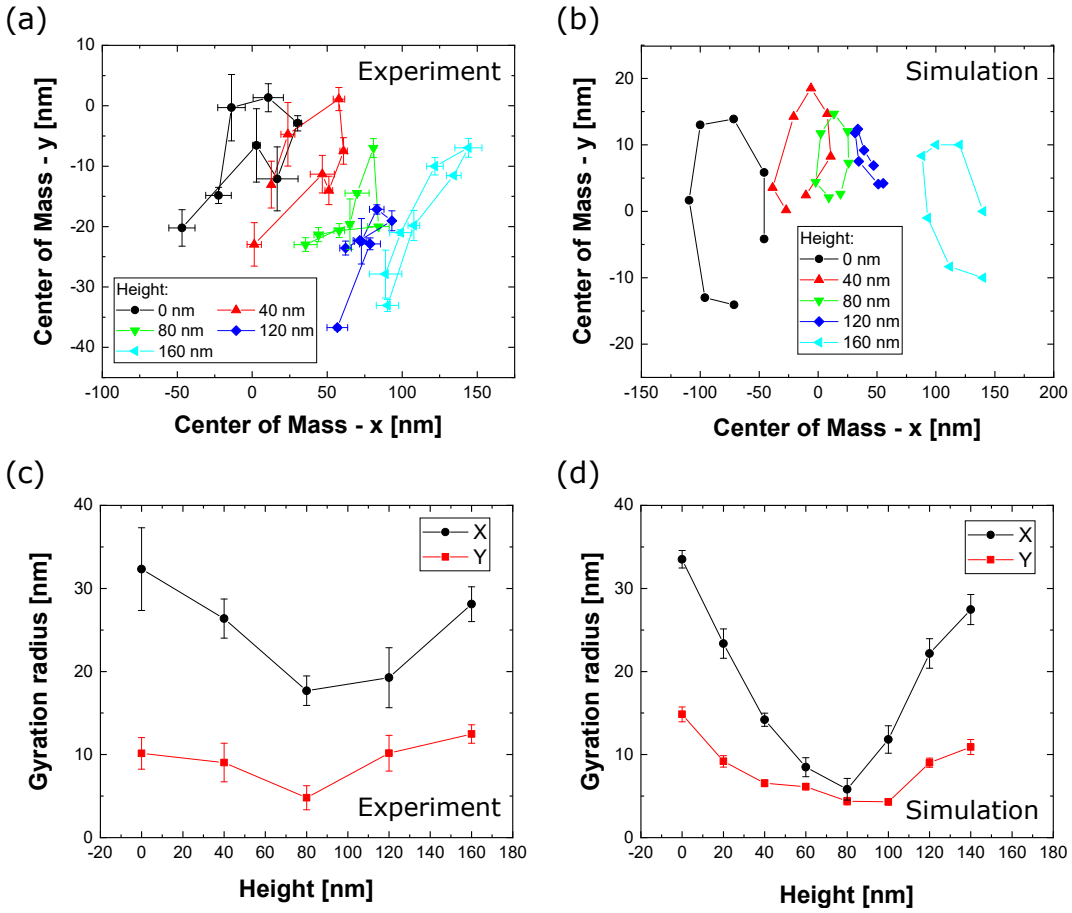

Figure 4: Experimental (a) and simulated (b) $x-y$ position of the vortex core's center of mass along the thickness of the CoFeB microstructured square. The fitted amplitude (sinusoidal fitting) of the $x-y$ vortex core gyration along the thickness of the CoFeB microstructured square is shown in (c) for the experimental data, and in (d) for the corresponding micromagnetic simulations.

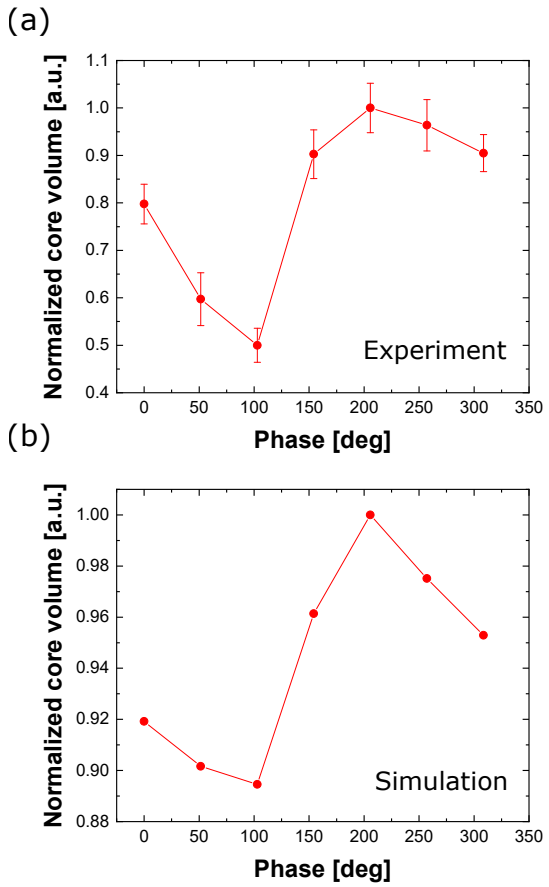

Figure 5: Temporal dependence of the vortex core volume, normalized to the maximum volume across an excitation cycle. (a) Experimental data. (b) Corresponding micromagnetic simulation.

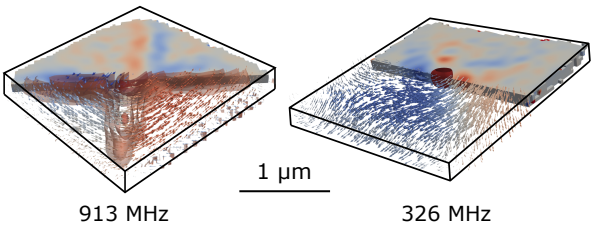

Figure 6: TOC graphic